# 7

# One dimensional simulation of CZTS heterostructure: Single & tandem junctions

## 7.1 Introduction

Kesterites have gathered considerable attention for future generation thin film technology. Suitable material's properties makes it a material of choice for next generation photovoltaic [Abermann, 2013]. However, recorded the maximum efficiency is near ~12% for kesterite based solar cells. No further improvement in efficiency is reported in last few years and the improvement is limited to the lab scale only [Takuya Kato, Homare Hiroi, Noriyuki Sakai, Satoshi Muraoka, 2012] [Lee et al., 2015]. Several factors such as large voltage deficit due to improper interface band alignment, inferior material quality due to difficulty in pure phase formation; formation of back contact barrier due to improper back contact etc. have been attributed to the observed efficiency loss in these cells. The kesterite solar cell device structure Al:ZnO/i-ZnO/CdS/CZTS,Se/Mo/SLG is adopted from its chalcopyrite (CIGS) counterpart due to its similar crystal structure and electronic properties [Chiril et al., 2011]. The high current with low voltage tradeoff for single bandgap absorber limits the performance of a single junction solar cell. Implementation of tandem cell structure in kesterite can be beneficial for the efficiency improvement.

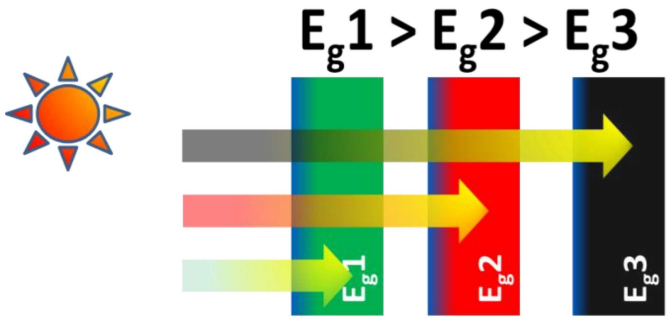


**Figure 7.1** Schematic representation of multijunction solar cell

The tandem or multi-junction solar cell structures, **Figure 7.1** utilize stacking of higher bandgap cell at the top followed by lower bandgap cells subsequently. The stacking of cells is made in such a way that high energy portion of the solar spectrum is absorbed in the top cell which remains transparent to the lower energy photons. The leftover solar spectrum is absorbed consecutively in lower cells of bandgap equivalent to the energy of photons. Multijunction solar cell with III-V compound semiconductors are already in use for space applications [Sayad, 2016]. Recently tandem cell structures with chalcopyrite absorbers is fabricated where $CuGaSe_2$ (CGS) (Eg ~ 1.7 eV) serves as top cell and CIGS (Eg ~ 1.14eV) is used as a bottom cell. A tandem cell efficiency of 7.2% is obtained with short circuit current density (Jsc) and open circuit voltage (Voc) ~ 10.6 mA/cm$^2$ and 1.18 V, respectively [Nishiwaki, Siebentritt, Walk, & Lux-Steiner, 2003]. In a similar way, tandem structure with $Ag(In_{0.2}Ga_{0.8})Se_2$ (AIGS) (Eg ~ 1.7 eV) top cell is used with CIGS as a bottom cell and the maximum efficiency of ~ 8% has been achieved with Jsc

and Voc equal to 9.1 mA/cm² and 1.3V, respectively [Tokio Nakada et al., 2007]. This chapter focuses on the simulation of CZTS/Se single and double junction tandem solar cell structures using one dimensional solar cell simulation program SCAPS-1D. First, a single junction CZTS/Se solar cell structure is optimized with different material and device parameters such as absorber thickness, carrier concentration, defects etc. Further, a double junction tandem structure is realized with CZTS top cell and CZTSe bottom cell for enhanced efficiency and the maximum efficiency of ~ 22% has been demonstrated.

## 7.2 Materials' properties and simulation approach

The kesterite solar cell device structure, Al:ZnO/ZnO/CdS/Absorber layer/Back contact, **Figure 7.2 (a)**, considered in this simulation includes CZTS and CZTSe as the p- type absorbers on the top of metallic back contact. A heterostructure junction is formed with an n-type wide bandgap CdS buffer layer. A thin wide bandgap intrinsic ZnO layer acts as a window layer, and simultaneously serves as a passivation layer for lower layers. Al doped ZnO (Al:ZnO) acts as a transparent conducting oxide (TCO) layer and serves as the front contact. The materials' properties considered in the simulation are summarized in **Table 7.1**. The optical absorption spectra for CZTS and CZTSe absorber are taken from literature [Adachi, 2015b] and for CdS and ZnO are used from the absorption spectra provided by SCAPS. These absorption spectra are shown in **Figure 7.2 (b)** for reference. Considering actual absorption spectrum for the materials is more realistic than considering a constant value and thus, will provide a better insight to the device performance.

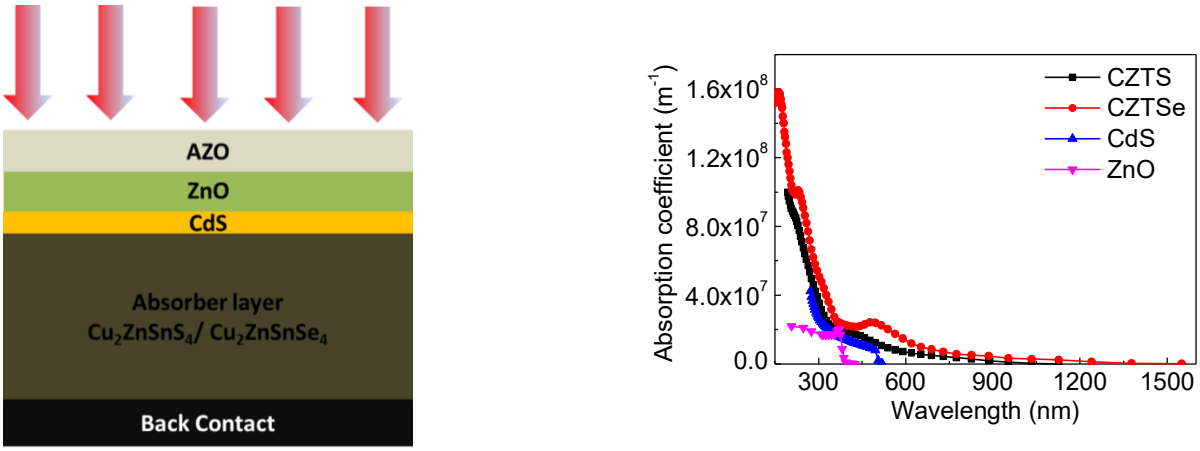


**Figure 7.2** (a) Schematic representation of "Al:ZnO/ZnO/CdS/*Absorber layer*/Back contact" single junction solar cell structure, used for simulating the device performance and (b) the absorption coefficients of different materials used in the present work

**Table 7.1** Material parameters, used in the present work for simulating single junction and tandem solar cell structures

| Material properties | CZTSe | CZTS | CdS | i-ZnO | Al:ZnO |
|---|---|---|---|---|---|
| Thickness [μm] | 2 | 2 | 0.05 | 0.08 | 0.2 |
| Bandgap [eV] | 1 | 1.5 | 2.42 | 3.37 | 3.37 |
| Electron Affinity [eV] | 4.46[Adachi, 2015a] | 4.3[Adachi, 2015a] | 4.5 | 4.6 | 4.6 |
| Dielectric permittivity | 9.1[Adachi, 2015b] | 6.95[Adachi, 2015b] | 9[Courel, Pulgaran-Agudelo, Andrade-Arvizu, & Vigil-Galan, 2016] | 9[Courel, Pulgaran-Agudelo, et al., 2016] | 9[Courel, Andrade-Arvizu, & Vigil-Galán, 2015] |
| Density of states in CB [$cm^{-3}$] | 2.2 x $10^{18}$ | 2.2 x $10^{18}$ | 1.8x$10^{19}$[Courel, Pulgaran- | 2.2 x $10^{18}$[Courel, | 2.2 x $10^{18}$ |

| | | | | | |
|---|---|---|---|---|---|
| | | | Agudelo, et al., 2016] | Pulgaran-Agudelo, et al., 2016] | |
| Density of states in VB [$cm^{-3}$] | 1.8 x $10^{19}$ | 1.8 x $10^{19}$ | 2.4x$10^{18}$[Courel, Pulgaran-Agudelo, et al., 2016] | 1.8 x $10^{19}$[Courel, Pulgaran-Agudelo, et al., 2016] | 1.8 x $10^{19}$ |
| Thermal velocity of electron [cm/s] | 1 x $10^{7}$ | 1 x $10^{7}$ | 1 x $10^{7}$ | 1 x $10^{7}$ | 1 x $10^{7}$ |
| Thermal velocity of hole [cm/s] | 1 x $10^{7}$ | 1 x $10^{7}$ | 1 x $10^{7}$ | 1 x $10^{7}$ | 1 x $10^{7}$ |
| Electron mobility [$cm^2$/Vs] | 145 | 100 | 160 | 150 | 150 |
| Hole mobility [$cm^2$/Vs] | 40 | 35 | 50[Courel, Pulgaran-Agudelo, et al., 2016] | 25[Courel, Pulgaran-Agudelo, et al., 2016] | 25[Courel et al., 2015] |
| Donor concentration [$cm^{-3}$] | 0 | 0 | 1 x $10^{17}$ | 1 x $10^{17}$ | 1x$10^{20}$ |
| Acceptor concentration [$cm^{-3}$] | 5 x $10^{16}$ | 5 x $10^{16}$ | 0 | 0 | |
| Absorption coefficient [$cm^{-1}eV^{1/2}$] | file[Adachi, 2015b] | file[Adachi, 2015b] | SCAPS | SCAPS | |
| Radiative recombination coefficient [$cm^{-3}$/s] | 1.04 x $10^{-10}$ | 1.04 x $10^{-10}$ | 1.04 x $10^{-10}$ | 1.04 x $10^{-10}$ | |
| Effective mass electron | 0.07 | 0.18[Courel et al., 2015] | 0.25[Courel, Pulgaran-Agudelo, et al., 2016] | 0.275[Courel, Pulgaran-Agudelo, et al., 2016] | 0.275[Courel et al., 2015] |
| Effective mass hole | 0.2 | 0.71[Courel et al., 2015] | 0.7[Courel, Pulgaran-Agudelo, et al., 2016] | 0.59[Courel, Pulgaran-Agudelo, et al., 2016] | 0.59[Courel et al., 2015] |
| Hole capture cross section ($cm^2$) | 1x $10^{-15}$ | 1x $10^{-15}$ | 1x $10^{-13}$ | 1x $10^{-15}$ | 1x $10^{-15}$[Courel et al., 2015] |
| Electron capture cross section ($cm^2$) | 1x $10^{-15}$ | 1x $10^{-15}$ | 1x $10^{-15}$ | 1x $10^{-15}$ | 1x $10^{-15}$ |
| Minority carrier lifetime | 5 ns | 10 ns | | | |
| Interface recombination speed (cm/s) | $10^3$[Courel, Andrade-Arvizu, & Vigil-Galán, 2016] | $10^4$[Courel, Andrade-Arvizu, et al., 2016] | | | |
| Defect type at bulk/interface | Donor/Neutral | Donor/Neutral | | | |

The proposed kesterite device structures are simulated using the one dimensional numerical simulator SCAPS [Burgelman & Decock, 2016], where coupled Poisson and continuity equations for both electrons and holes are solved with suitable boundary conditions [Burgelman & Decock, 2016]. In the device simulation, donor defects are introduced at 0.6 eV above valence band of absorber layer and neutral defects at 0.6 eV above valence band is considered at absorber layer/CdS heterointerface. The defect energy level are taken sufficiently deep in the bandgap to ascertain mid gap defects. The work function of back contact is replicated as Mo by considering its equal to Mo i.e. 5 eV. Electron and hole surface recombination speeds are taken equal to 1 x $10^5$ cm $s^{-1}$ and 1 x $10^7$ cm $s^{-1}$, respectively at the back contact. Thermionic emission and radiative recombination are considered for the transport properties of majority charge carriers with recombination coefficient equal to 1.04 x$10^{-10}$ $cm^3s^{-1}$ for all the layers in the simulation [Simya, Mahaboobbatcha, & Balachander, 2015]. Auger recombination is not considered in this simulation as it is significant only at higher carrier concentrations. For

simplicity of calculations, capture cross section and thermal velocity are kept same $10^{-15}$ $cm^2$ and $10^7$ cm/s for electron and holes, respectively. The minority carrier life time at the bulk of absorber layer and the interface recombination speed at absorber/buffer layer interface are taken 10 ns, $10^4$ cm $s^{-1}$, and 5 ns, $10^3$ cm $s^{-1}$ for CZTS and CZTSe absorbers, respectively [Courel, Andrade-Arvizu, et al., 2016]. This assumption for the base device falls well within the range of the mostly reported kesterite devices.

## 7.3 Device analysis for a single junction solar cell with CZTS and CZTSe absorber layers

The estimated band alignments and the current voltage characteristics are shown in **Figure 7.3** for the single junction solar cell device with CZTS and CZTSe absorber. A spike is observed in the band alignment at CZTS/CdS interface. A large cliff and spike in the band structure will lower the open circuit voltage and short circuit current density (Jsc), respectively. Hence optimization of heterostructure interface is necessary for enhanced performance. The large short circuit current density and high open circuit voltage is obtained with CZTSe and CZTS absorber cell, respectively. This can be understood by the computed quantum efficiency plots, shown in the inset of **Figure 7.3 (b)**. Large area is covered in the quantum efficiency curve for lower bandgap CZTSe absorber thereby increasing the short circuit current density. Large open circuit voltage of CZTS device corresponds to its relatively larger bandgap. The optimal photovoltaic efficiencies computed with the considered device structure are ~ 13.41% and 14.88% for single junction CZTS and CZTSe solar cell, respectively. The respective device parameters are summarized in a table in the inset in **Figure 7.3 (b)**.

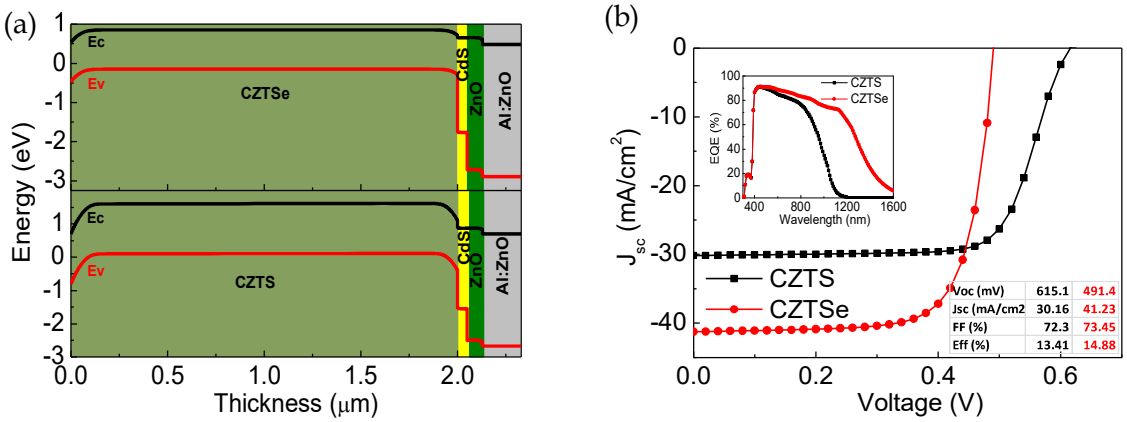


**Figure 7.3** (a) Band alignment at the interface and (b) Current-voltage (I-V) characteristics of single junction CZTS and CZTSe solar cells.

### 7.3.1 Impact of absorber layer thickness on single junction photovoltaic performance

The impacts of absorber layer thickness on the considered device structure are summarized in **Figure 7.4**. The open circuit voltage for CZTS device, **Figure 7.4 (a)** is relatively large compared to CZTSe device because of its high bandgap. The open circuit voltage is relatively immune to the thickness and slight increase in it corresponds to the increase in majority carrier due to the enhanced absorption. The increase in thickness offers enhanced absorption according to Beer-Lamberts law $I = I_0 e^{-\alpha x}$ and results into enhanced photo generated current density **Figure 7.4 (b)**. The cumulative effect of enhanced open circuit voltage and the short circuit current density is reflected in the efficiency plot, shown in **Figure 7.4 (c)**. The quantum efficiency curve, **Figure 7.4 (d)** covers large area for the CZTSe absorber because of its lower bandgap and results into high short circuit current density at same thickness as compared to CZTS absorber cell.

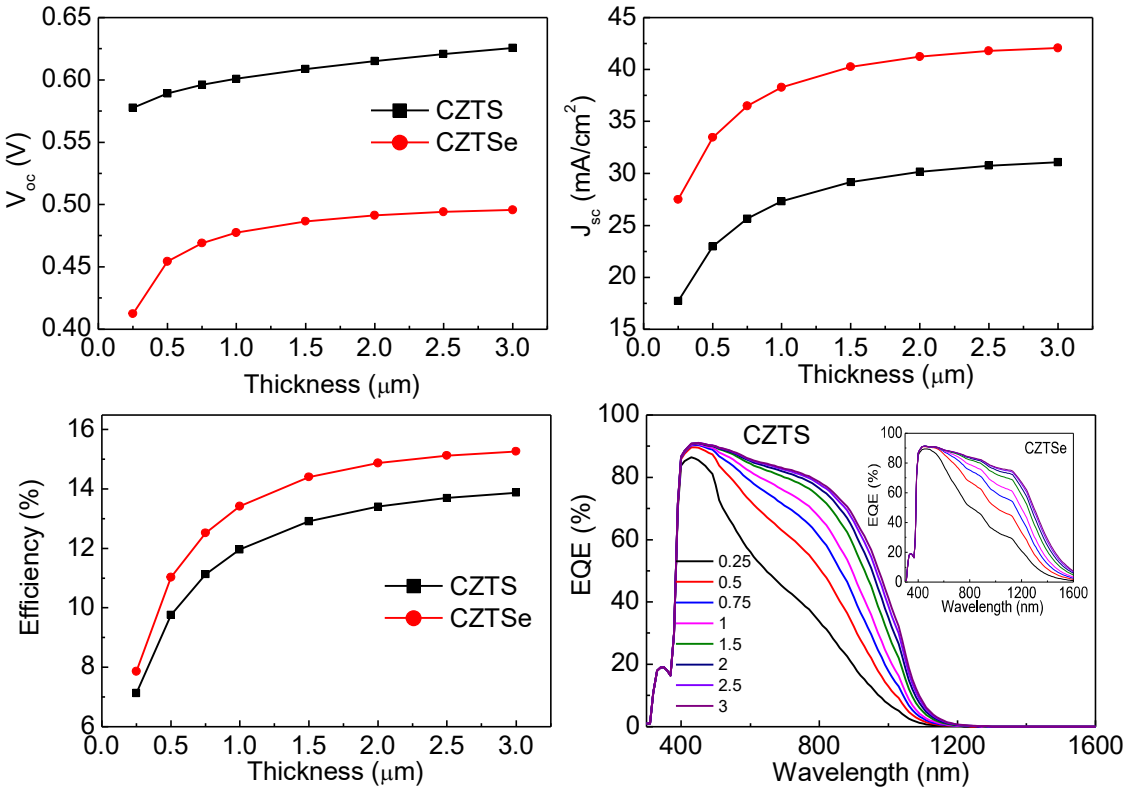


**Figure 7.4** (a) Open circuit voltage; (b) short circuit current density; (c) efficiency, and (d) quantum efficiency of CZTS and CZTSe absorber solar cells at different absorber layer thickness.

### 7.3.2 Impact of absorber layer acceptor concentration on single junction photovoltaic performance

CZTS/Se is an intrinsic p type absorber due to non-stoichiometry and defects present in it. The hole concentration in the absorber layer is varied from 1 x$10^{12}$ $cm^{-3}$ to 1 x$10^{18}$ $cm^{-3}$ in the simulation. The computed open circuit voltage, Voc, **Figure 7.5 (a)**, and the short circuit current density, Jsc, **Figure 7.5 (b)**, increases steadily and then starts decreasing, with increasing the hole concentration. The calculated results are in agreement with the fact that increased carrier concentration results in increased carrier recombination thereby reduces the minority carrier life time. Further, increased carrier concentration causes reduced depletion width inside the absorber layer which affects the effective separation of photo generated charge carrier thereby reduces the short circuit current density. The simulated efficiency versus acceptor density results shown in **Figure 7.5 (c)** suggest that the optimal carrier density is up to 5 x $10^{16}$ $cm^{-3}$ for CZTS and 1 x $10^{17}$ $cm^{-3}$ for CZTSe solar cell. The calculated maximum efficiency, Voc and Jsc with these carrier densities are ~13.41%, 615 m V and 30.15 mA/$cm^2$, respectively for CZTS and ~15.6%, 514.29 mV, 40.52 mA/$cm^2$ for CZTSe solar cell, respectively.

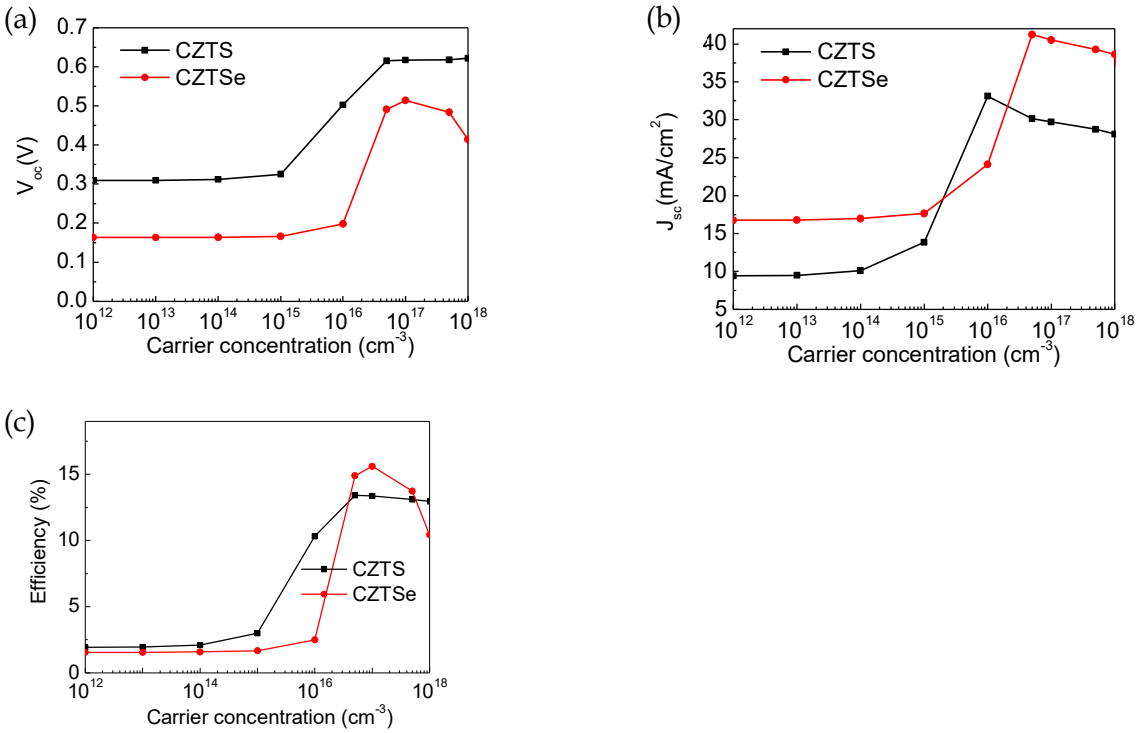


**Figure 7.5** (a) Open circuit voltage; (b) short circuit current density; and (c) efficiency at different hole concentration for CZTS and CZTSe absorber based solar cells.

### 7.3.3 Impact of defect concentration at absorber and at absorber/CdS interface

CZTS,Se is a defect prone system with relatively lower formation energy for acceptor defects, making it an intrinsic p-type semiconductor. In present simulation, we considered single donor defect in bulk of the absorber layer and neutral defects at absorber/CdS interface. The defects are considered at mid band with characteristic energy level at 0.6 eV above valance band. The change in efficiency is summarized in **Figure 7.6 (a, b)** against absorber and absorber/CdS interface defect concentrations, respectively. It is observed that for moderate defect concentrations, especially in absorber, the efficiency is not changing significantly. This is probably due to the lower defect photogenerated carrier scatterings because of lower defect concentration and thus, not affecting the device performance. However, after certain defect concentration, in the range of high $10^{16}$ $cm^{-3}$, the efficiency drops drastically to the very low values, close to zero for both CZTS and CZTSe absorbers. In contrast, absorber/CdS interface defects seem more prone in degrading the photovoltaic performance and a slight increase in interface defect concentration resulted in reduced photovoltaic efficiency, **Figure 7.6 ( b)**. Thus, absorber/buffer interface defects should be minimized as much as possible to realize the enhanced photovoltaic efficiency. The presence of defects in the bulk determines the lifetime of minority carrier in the absorber while defects at the interface determine the recombination speed (S) at the interface. The impact of minority carrier life time and the interface recombination speed are simultaneously observed in the contour plot shown in **Figure 7.6 (c)** and **Figure 7.6 (d)** for CZTS and CZTSe, respectively. These results suggest that the higher minority carrier life time and low interface recombination are necessary to realize high efficiency for both CZTS and CZTSe absorbers.

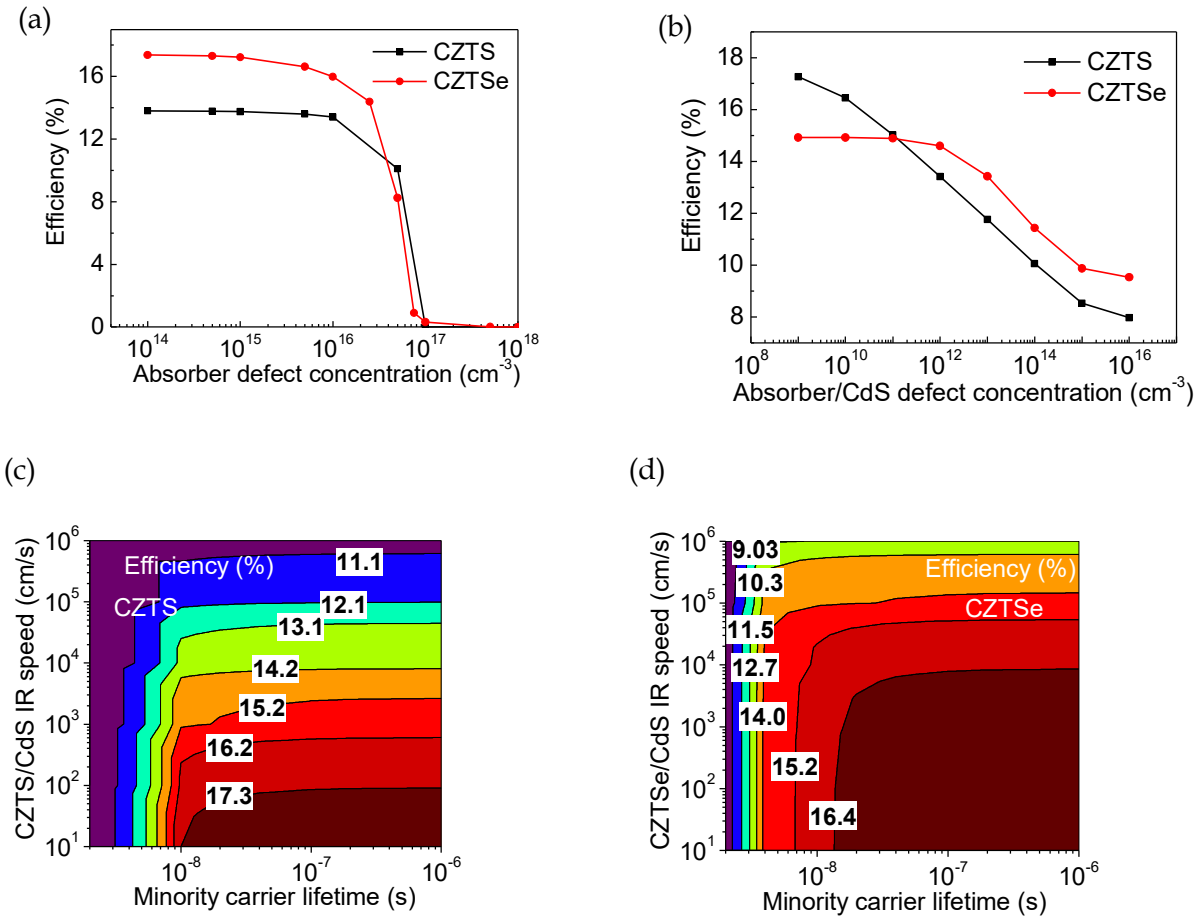


**Figure 7.6** Impact of defect concentration (a) and absorber/CdS interface defect concentration (b) in efficiency for CZTS and CZTSe solar cells and contour plots showing variation of efficiency with minority carrier life time and interface recombination speed in CZTS (c); and CZTSe (d).

### 7.3.4 Impact of buffer layer

The heterostructure device efficiency dependents critically on the band alignment at heterojunction interface. CdS is widely used buffer layer with CZTS/Se devices. The thickness of the buffer layer is related to its conductivity. To consider their impact on the device performance, carrier concentration of the buffer layer is simultaneously varied with its thickness and the computed solar cell efficiency is plotted in **Figure 7.7 (a)** and **Figure 7.7 (b)** for CZTS and CZTSe solar cells, respectively. The results suggest that solar cell performance is relatively insensitive to the buffer layer thickness and increases with increasing carrier concentration of buffer layer.

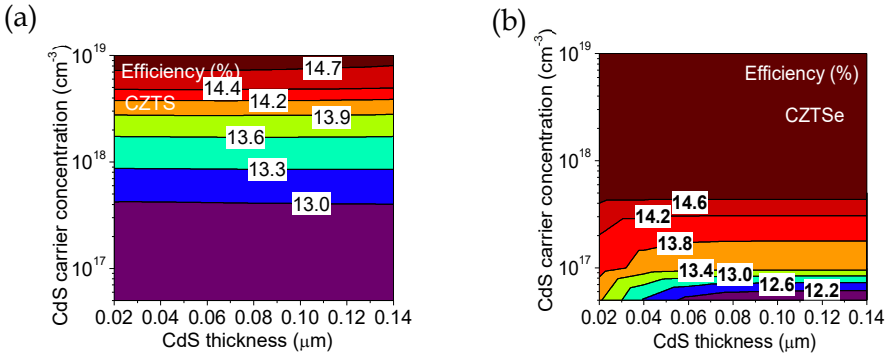


**Figure 7.7** Impact of CdS buffer layer thickness and carrier concentration on CZTS (a) and CZTSe (b) solar cell efficiency

The conduction band offset (CBO) at the absorber/buffer heterojunction interface plays an important role in governing the carrier transport through the junction. The offset in the conduction band is determined by the difference in electron affinities of absorber and buffer layer. A positive band offset results in the spike, whereas cliff is noticed for negative band offset at interfaces in the heterostructure devices. To see the impact of conduction band offset electron affinity of CdS layer is varied and the corresponding band alignment with observed conduction band offset is shown in **Figure 7.8 (a, b**) for CZTS and CZTSe solar cells.

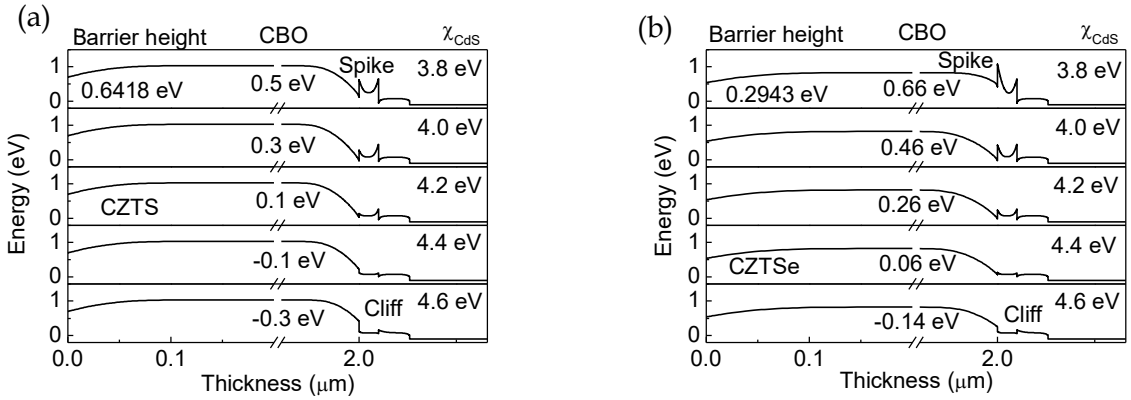


**Figure 7.8** Conduction band offset (CBO) in (a) CZTS (b) CZTSe at different CdS layer electron affinity ($\chi_{CdS}$)

It is observed that a cliff type band offset results in a decreasing open circuit voltage, **Figure 7.9 (a)** while short circuit current remains relatively unchanged, **Figure 7.9 (b)** except at very low CdS electron affinity values. Further, the efficiency versus CdS electron affinity variation is summarized in **Figure 7.9 (c)**, showing inverted U shaped behavior. Thus, a moderate buffer layer electron affinity, closer to electron affinity of absorber layer in the range 4.0 eV – 4.4 eV, is essential to realize the maximum efficiency for both CZTS and CZTSe absorber based photovoltaic devices.

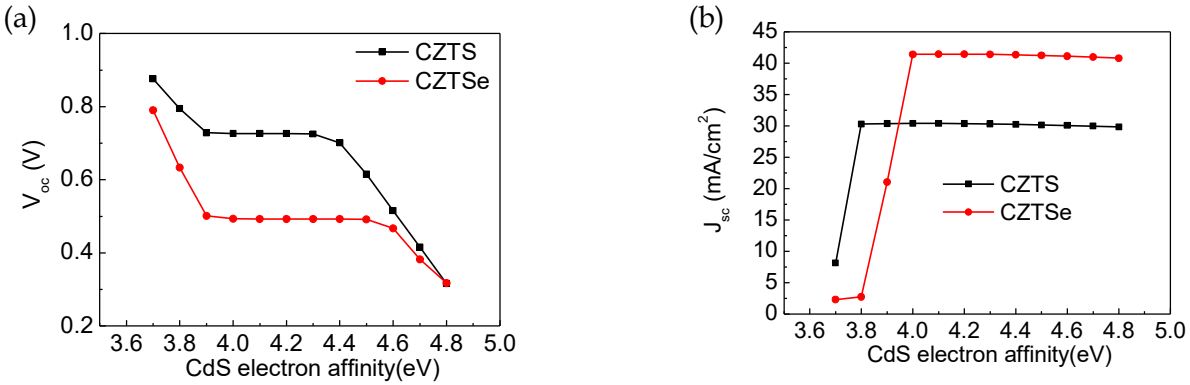

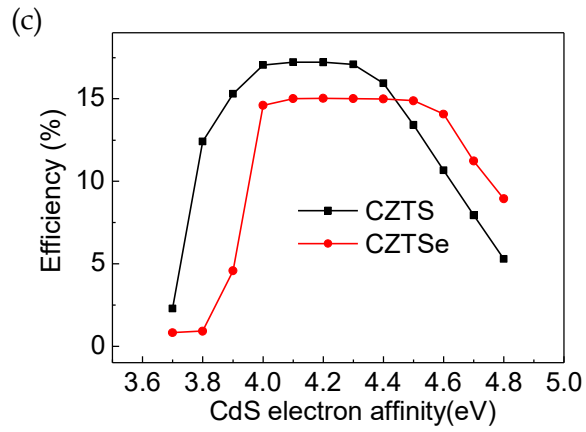


**Figure 7.9** Impact of CdS electron affinity (band offset at absorber/CdS interface) on Voc (a); Jsc (b); and efficiency (c) for CZTS and CZTSe solar cells

We further observed that conduction band offset and interface recombination speed affect the device parameter and thus, are important parameters to decide the selection criteria for the suitable buffer layer for the optimal photovoltaic response. The computed device parameters are summarized in the contour plot in **Figure 7.10**. The contour plot for $V_{oc}$ **Figure 7.10 (a, b)** and $J_{sc}$, **Figure 7.10 (c, d)** suggest that cliff in the band structure ($\chi_{CZTS,Se} < \chi_{Buffer}$) reduces the open circuit voltage, whereas short circuit current density remains nearly insensitive for both CZTS and CZTSe solar cell. In contrast, $J_{sc}$ decrease with increase in spike ($\chi_{CZTS,Se} > \chi_{Buffer}$) in the band offset at the heterointerface. High interface recombination (IR) speed causes negative impact on the device performance and for optimum buffer layer, a minimum interface recombination speed is suggested.

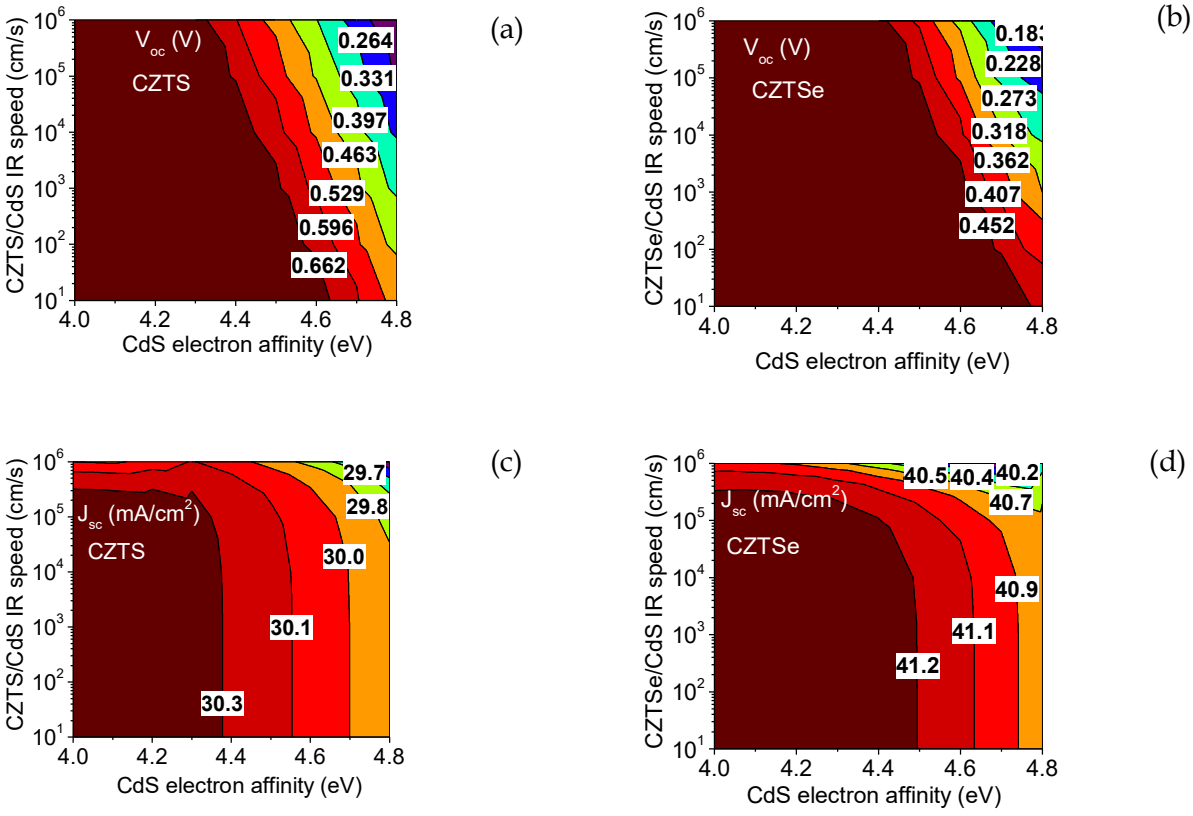

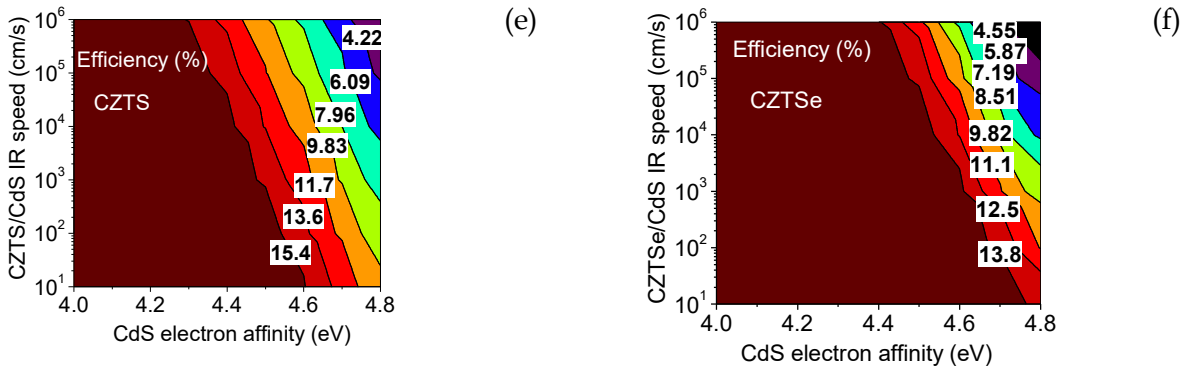


**Figure 7.10** Impact of interface recombination speed and CdS electron affinity on (a) Voc, (c) Jsc, (e) and efficiency for CZTS and (b) Voc, (d) Jsc, and (f) efficiency for CZTSe absorber based devices.

### 7.3.5 Impact of Back contact work function

Mo is a widely used back contact material with CZTS/Se solar cells. However, its effectiveness is still not well understood, as it forms a non-ohmic back contact with the absorber. High metal work function is required to form ohmic contact with the absorber layer. Here in present simulation, we varied the metal work function from 4.4 to 5.5 eV and the results are summarized in **Figure 7.11**. The low metal work function causes large barrier height at the back contact junction and thus, hampers the open circuit voltage and short circuit current of the device as shown in **Figure 7.11 (a)**. In contrast, high metal work function enhances the device efficiency, **Figure 7.11 (b)** by forming ohmic back contact. These results suggest that a metal with work function above 5.3 eV for CZTS and above 5 eV for CZTSe is essential for realizing high efficiency devices.

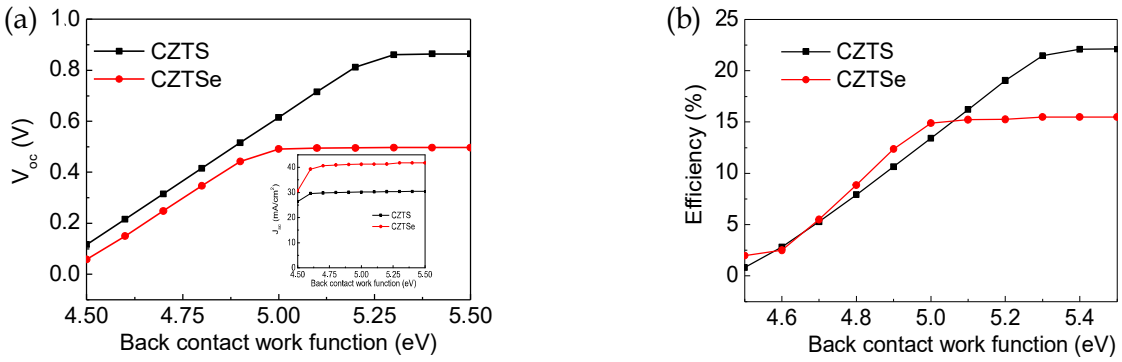


**Figure 7.11** Impact of metal work function on Voc (inset Jsc) (a) and efficiency (b) for CZTS and CZTSe solar cell

### 7.3.6 Design and analysis of CZTS/CZTSe tandem solar cell structure photovoltaic device

Single junction solar cell efficiency is limited to SQ limit with the respective absorber bandgap values. The efficiency of the solar device can be improved by realizing the tandem structure with high bandgap top cell fabricated over a current matched lower bandgap bottom cell. Here, we consider CZTS/CZTSe tandem cell structure, **Figure 7.12** and calculated the tandem cell device performance by matching the short circuit current density of the top and bottom cell. The tandem cell structures can be fabricated using monolithic integration of one cell on the top of other cell [Nishiwaki et al., 2003]. An n+/p+ tunnel junction at the interface is essential to overcome the reverse bias issues of the two cells for proper current flow across the tandem structure. The transparent materials such as indium tin oxide (ITO), fluorine doped tin oxide (FTO), aluminum doped zinc oxide (AZO), molybdenum doped indium oxide (IMO) with high mobility can serve well in making a tunnel junction between the top and bottom cells. Tokio Nakada et al. fabricated chalcopyrite tandem solar cell with $Ag(In_{0.2}Ga_{0.8})Se_2$ (AIGS)

upper cell on top of the transparent IMO and CIGS as the bottom cell. This tandem structure showed ~ 8% photovoltaic efficiency with 1.3V open circuit voltage [Tokio Nakada et al., 2007].

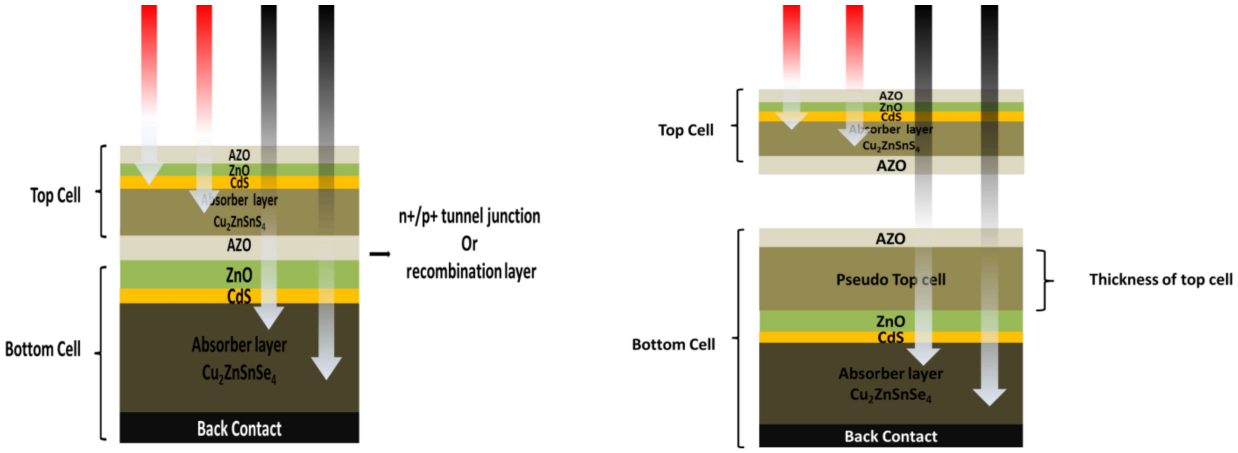


**Figure 7.12** Schematic representation of tandem cell structure with CZTS top cell and CZTSe bottom cell in conjunction with tandem connections

The top and bottom cells are simulated separately first to simulate tandem structure in SCAPS. Further, a pseudo top cell is considered for simulating the bottom cell with equivalent thickness as original top cell is placed on the bottom cell to ensure the bottom cell is illuminated with equivalent remaining solar spectrum, after equivalent absorption in the top cell. The electron affinity of pseudo CZTS top cell is taken such that there is no band discontinuity. The defect density in pseudo CZTS absorber layer is taken sufficiently high to ensure the low minority carrier life time such that high energy solar spectra (hν > 1.5 eV) do not contribute to the photocurrent characteristics of bottom cell.

The maximum current of a tandem cell is limited by the minimum current from the individual subcells while the maximum open circuit voltage is the sum of open circuit voltage of the individual cells. To ensure individual subcells do not limit the current conduction, the short circuit current density of constituent cells is matched. The current matched conditions for the tandem structure are obtained at the point of intersection of top and bottom cell current densities, as shown in **Figure 7.13 (a)**. The computed thicknesses for matched short circuit current values are summarized in **Figure 7.13 (b)**. It is observed that the current matching condition can be obtained at relatively lower CZTS top cell thickness as compared to the bottom cell thickness. The tandem cell performance increases with increasing the bottom CZTSe cell thickness, as observed in the computed Jsc and Voc curves, shown in **Figure 7.13 (c).**

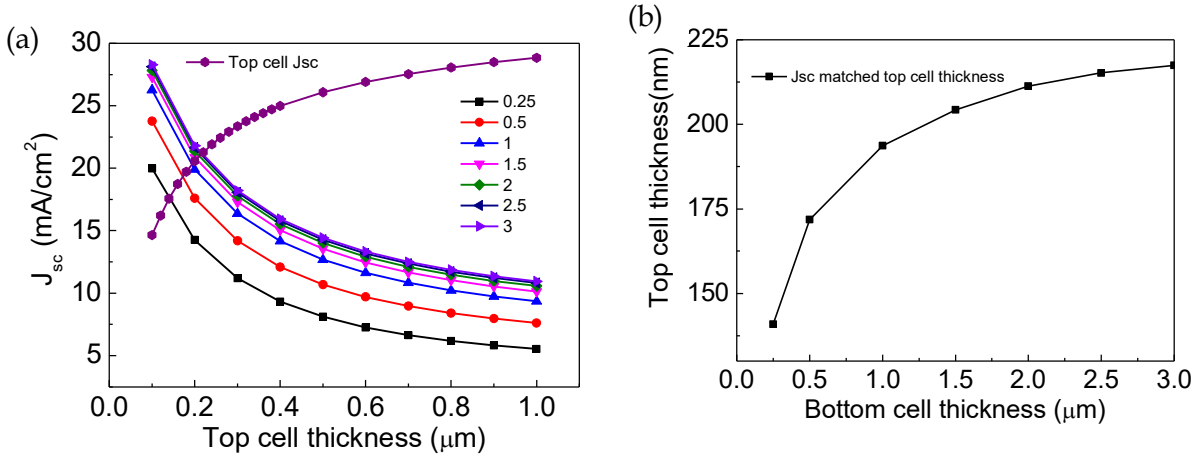

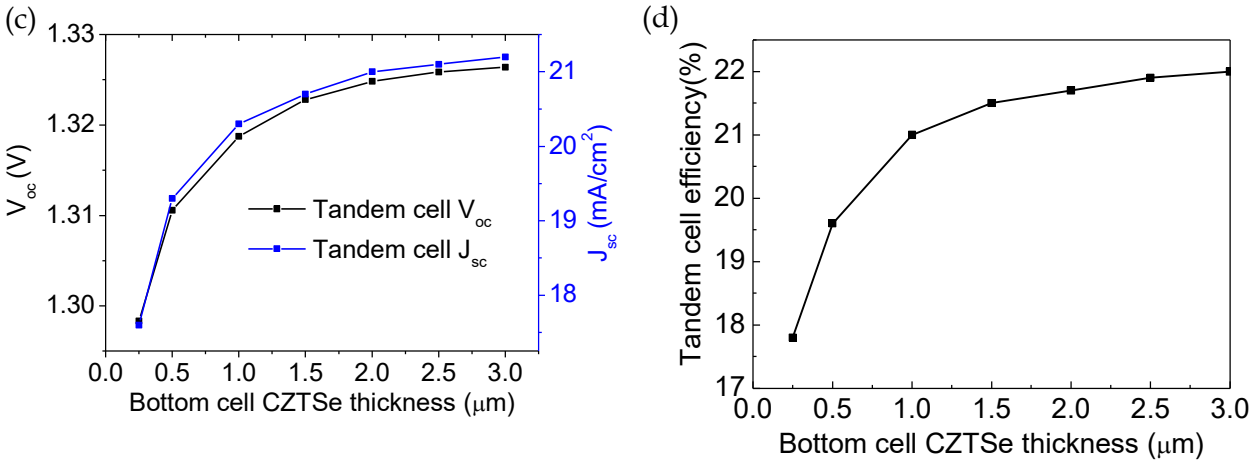


**Figure 7.13** (a) Variation of current density of CZTS top cell and CZTSe bottom cell at different thicknesses (b) Thickness of top CZTS cell matched with different thickness of bottom CZTSe cell (c) Current density and open circuit voltage curve for tandem structure with current matched top and bottom cell at different bottom cell thickness (d) Tandem structure efficiency at different bottom cell thickness.

The noticed increase in short circuit current density is attributed to the enhanced absorption of solar energy causing enhanced photo generated carrier in the device. The open circuit voltage of the tandem cell remains relatively immune to the thickness of the cell. The tandem cell efficiency as a function of bottom cell thickness is shown in **Figure 7.13 (d)** under current matching condition. We observed that the tandem cell efficiency increases with cell thickness and saturates at or above 2μm thick bottom cell. The current - voltage characteristics and the quantum efficiency of the tandem structure with 2μm thick CZTSe bottom cell and 211nm thick matched CZTS top cell are shown in **Figure 7.14 (a, b).** We observed that the top CZTS and bottom CZTSe cells show enhanced absorption in the low and high wavelength region of the solar spectrum corresponding to their respective bandgap. This tandem structure, thus results in photo current generation in wide spectral range as shown in the quantum efficiency curve **Figure 7.14 (b).** The estimated tandem cell device parameters are listed in **Table 7.2** for top, bottom and tandem cell structures. The maximum efficiency achieved is about 21.7% for the optimized tandem CZTS/CZTSe solar cell structure in the investigated device configuration.

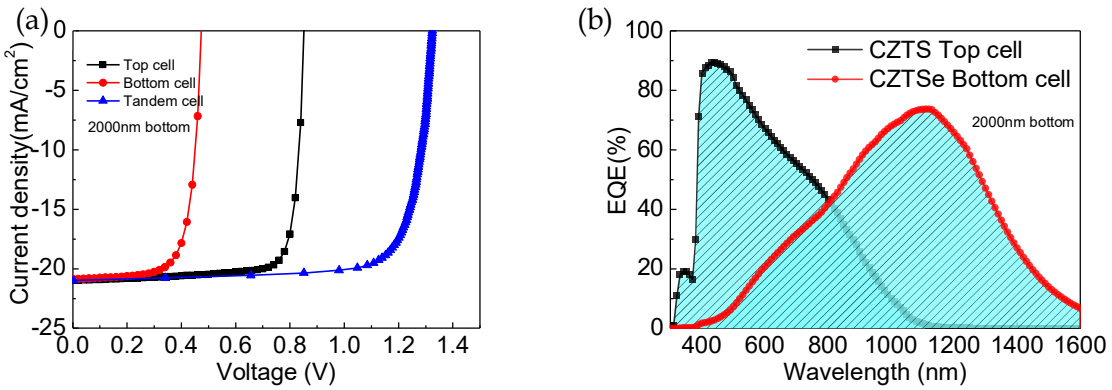


**Figure 7.14** (a) Current-voltage characteristics and (b) quantum efficiency for CZTS top cell CZTSe bottom cell and CZTS/CZTSe tandem cell

**Table 7.2** CZTS and CZTSe cell performance with single cell and in the tandem configuration

| | Jsc ($mA/cm^2$) | $V_{oc}$ (mV) | FF (%) | Efficiency (%) |
|---|---|---|---|---|
| 211.33nm CZTS single cell | 20.98 | 852.9 | 81.95 | 14.67 |
| 2 μm CZTSe single cell | 41.73 | 496.6 | 74.61 | 15.46 |
| CZTS Top cell in tandem structure | 20.98 | 852.9 | 81.95 | 14.67 |
| CZTSe Bottom cell in tandem structure | 20.87 | 474.1 | 72.59 | 7.18 |
| Tandem cell | 20.98 | 1324.82 | 78.2 | 21.7 |

This proposed tandem structure simulation suggests that CZTS and CZTSe can serve efficiently as a top and bottom cell for the tandem structure with maximum efficiency ~ 21.7% under current matched condition. The noticed open circuit voltage and short circuit current values are ~ 1.33 V and ~ 20.98 mA $cm^{-2}$, respectively for the investigated tandem solar cell.

## 7.4 Conclusion

Kesterite CZTS/Se solar cells are investigated using one dimensional SCAPS 1D solar cell simulator. Single junction and the possible double junction tandem structure are investigated for the optimized device performance. The single junction device performance critically depends on the band alignment at the heterojunction interface. The presence of defects in bulk and at absorber/CdS interface degrades the device performance. Additionally, a high work function metal may serve more efficiently as a back contact in place of Mo, making ohmic back contact with CZTS/Se. The proposed tandem structure shows potential realizing enhanced the photo conversion efficiency for kesterite devices with efficiency reaching up to~ 22%. Further improvement can be possible by introducing a higher band gap kesterite such as $Cu_2ZnGeS_4$ in the top cell of the tandem structure.